

# **SIMPLIFIED DESCRIPTION OF OPTICAL GYROS – A RIGOROUS ANALYTICAL DEVELOPMENT WITHOUT VECTOR CALCULUS**

**Paul G. Savage**

Strapdown Associates, Inc.  
Maple Plain, MN 55359 USA

WBN-14027

[www.strapdownassociates.com](http://www.strapdownassociates.com)

May 23, 2020 (Updated April 8, 2024)

## **ABSTRACT**

Ring laser gyros (RLGs) and fiber optic gyros (FOGs) measure angular rotation by the phase difference generated between oppositely directed monochromatic light waves traversing a closed optical waveguide embedded in the gyro structure. This article presents a simplified but comprehensive analytical development showing how the rotation induced phase difference is created at the gyro readout photo detector by two effects, 1} Wavelength difference between the oppositely directed waves caused by classical Euclidean geometrical effects (the same predicted by Special Relativity when rotation induced velocity of the waveguide is small compared to the speed of light), and 2} The speed of light being the same relative to the rotating gyro as it is in non-rotating inertial space, an exclusive property of Relativity. This contrasts with previous explanations attributing rotation induced phase shift to a difference in optical path length between the oppositely directed waves, or to a time difference for the oppositely directed waves to traverse the waveguide. These explanations, were with respect to non-rotating space, not to the rotating gyro readout used for angular rotation measurements. Relative to the readout, it is shown that the time for each of the oppositely directed waves to traverse the waveguide is the same.

This article first derives a general equation describing how rotation induces a change in optical power when the oppositely directed beams are combined to illuminate the readout detector. Applying the equation to an RLG shows how cyclic outputs are generated from the photo detector, each representing a known increment of angular rotation. Application to a FOG shows how successive angular rotation increments are measured, each over the time for the waves to traverse the fiber coil. Analysis of “closed-loop” FOG operations describes how to operate lithium–niobate crystals inserted in the fiber coil to balance rotation induced phase shift while generating angular rotation outputs.

## **FOREWORD**

This article is a simplified version of [1] designed for the technical reader with limited analytical background. As such, all analytical developments are based on simple algebra and trigonometry without resorting to vector calculus used in [1]. This is achieved by simplifying the

optical gyro wave path model to be circular. As rigorously demonstrated in [1], both fiber optic and ring laser gyros can be analytically represented by an equivalent circular wave path configuration.

## INTRODUCTION

Optical gyros (ring laser and fiber optic) have been in broad usage since the late 1970s. Curiously, however, their basic principle of operation has varied between designers and users. Optical gyros measure the change in phase induced by angular rotation in oppositely directed monochromatic light waves created within the gyro. Some attribute the phase change to Relativity theory while others characterize it as a classical kinematic Doppler effect. Many of these and other explanations have relied on heuristic reasoning to explain actual measured optical gyro operating characteristics. The purpose of this article is to provide a rigorous comprehensive analytic derivation of equations governing the operation of optical gyros and in the process, identify those attributed to classical vector kinematics, and those uniquely contributed by Relativity. The analysis is based on idealized optical gyro configurations in which oppositely directed light waves occupying the same physical space are independent from one-another, unaffected by imperfections in the closed waveguide directing their motion within the gyro, and having the same polarization direction when combined at the readout photo detector(s).

Relativity theory relates the motion of a point in space as measured by two remote observers in motion relative to one-another. When the velocity magnitude between observers is small compared to the speed of light, the observed motion forecasted by Special Relativity theory [2 Part 1; 3 Chpt VI; 4] reduces to classical Euclidean kinematic predictions [2 pp 37-38; 3 Chpt III Sect 7; 5 Sect 12-1]. Such is the case for optical gyros when analyzing how angular rotation impacts each of two oppositely directed light waves travelling within the gyro along a common closed optical path. Similar to the Doppler-like frequency shift observed in light waves emanating from receding stars, both Euclidean and Relativistic kinematics predict an angular rotation induced wavelength shift in the optical gyro light waves, increasing for the wave travelling in the direction of rotation, decreasing for the oppositely directed wave. Coupled with the wavelength shift, Relativity predicts that the propagation speed for each of the oppositely directed light waves will be the same “speed-of-light” relative to the rotating waveguide, the same as for light waves propagating through non-rotating inertial space. Light wave frequencies equate to the speed-of-light constant divided by their wavelength, thus, decrease for waves travelling with rotation and conversely for oppositely directed waves, generating a frequency difference between the oppositely directed waves. When the oppositely directed waves are mixed by the gyro readout, a combined beam power signal is generated whose intensity measures the rotation induced frequency difference. The combined beam power illuminates a readout photo detector, thereby generating a measurement of angular rotation. This is exactly what is produced in operating optical gyros under rotation, and what is predicted by the analytical development in this article.

Beginning from classical vector geometry, this article first analytically describes the distance vector to the same remote point in space as measured by each of two observers. Classical

Euclidean kinematics then describes how the observed remote point location is impacted by relative motion between the observers. The equivalent result is also derived in the Appendix based on Special Relativity theory, producing the same result when the relative velocity magnitude between observers is small compared to the speed of light.

Both the Euclidean and Relativity results are derived in non-rotating coordinates. The article then derives the equivalent in rotating coordinates by projecting the relative position vector geometry onto two non-rotating coordinate frames, one rotated from the other by a small angular rotation. The difference between the two projections is identified as the change that would be measured in a rotating coordinate frame undergoing the small angular rotation. Substituting the original non-rotating coordinate result, derives an equation relating the motion of the remote point as measured by one observer in non-rotating coordinates, in terms of the differential measurement taken by the other observer in rotating coordinates.

The analytical development to this point in the article is general in nature. Continued analysis specializes the two observation points to be fixed within a rigid body (a gyro), defining the observed point in motion to be a photon of light traversing a waveguide within the gyro, defining one of the observation points to be within the waveguide at the start of a photon's motion, the other at a reference "rotation center" external to the waveguide, with gyro rotation equated to that of the rotating coordinate frame. In the process, the photon in motion is defined to be part of a travelling light wave whose wavelength relative to the rotating gyro is a function of the wavelength in non-rotating space, the distance from the reference point to the photon, and the gyro's angular rotation during the time the photon traverses a wavelength of distance. The wavelength solution is then used to obtain independent integral solutions for each of the oppositely directed light waves traversing the gyro waveguide.

Combining the individual light wave solutions in the readout zone at the same instant of time (a common intersection in space/time) requires application of Relativity theory. The method is to first recognize that in a non-rotating frame, the wave propagation speed at any point in the waveguide will be at the same speed-of-light constant as it is open-space. Second, for the observer stationed in the rotating waveguide, the small movement of a passing photon, although rotated through a small amount, will (to first order in the rotation angle) be of the same magnitude as when measured in a non-rotating frame at the same location. By joining these observations, it is analytically shown that relative to the rotating waveguide, the propagation rate for each of the oppositely directed beams will be at the same speed-of-light, hence, the time interval for each wave to traverse a given distance relative to the waveguide will also be the same. Applying this finding to each of the oppositely directed waves allows them to be analytically summed (at a common space/time location) into a single equation defining the beam power that will illuminate the gyro readout photo detector(s). The result equates the cumulative difference in phase between the individual waves to the integrated effect of angular rotation over a selected time interval. For the remainder of the article, the combined beam power equation is used to explain the operating characteristics of fiber optic and ring laser optical gyros.

The ring laser gyro result analytically demonstrates how combining the oppositely directed waves at the gyro readout creates an optical interference pattern that moves across the photo detector(s) at a linear rate proportional to the gyro angular rate, thus generating cyclic outputs,

each representing a known increment of angular rotation. The fiber optic gyro result describes two types FOGs, those classified as “open-loop” and those classified as “closed-loop”. By injecting phase bias into the light waves with lithium-niobate (L/N) integrated-optics crystals inserted in the fiber coil, the closed-loop configuration provides control bias to the oppositely directed light beams that adds to the phase induced by angular rotation. Using outputs from the gyro photo detector, L/N bias command equations are derived to balance the rotation induced phase, while simultaneously generating successive outputs of gyro angular rotation over the time interval for a light wave to traverse the fiber coil.

The more detailed FOG L/N bias routines in [1] include provisions to eliminate round-off error generated by three closed-loop electronics interface operations; 1) Digitally sampling photo detector analog measurements into the digital control loop processor, 2) Creating L/N analog bias control voltages from the digital control-loop processor, and 3) Converting angular rotation increments calculated in the control-loop processor for digital output format compatibility.

## NOTATION

The following general notation is used in the article:

$/i$  = Subscript denoting the parameter being observed (measured) at position location point  $i$ .

$k(t)$  = A particular location in space/time at general spatial position point  $k$  at time  $t$ .

Observable Event = An event at a position location in space at a particular instant of time (e.g., a lightning strike, explosion, illumination by a radar pulse, or passage of the leading edge of a light wave across a point in space) that can be observed at a remote spatial location based on electro-magnetic wave propagation (e.g. light or radar) [2 pp 29, 36; 3 pp 28, 236-238; 6 pp 10].

## DIFFERENTIAL POSITION MOTION

Consider a circularly shaped optical gyro wave path of radius  $r$ , e.g., a fiber optic gyro or the analytical equivalent of a circle inscribed within a symmetrical ring laser gyro that is tangent to each leg. Define point  $a$  to be at the center of the circle and another point  $i$  fixed to the gyro in the wave path. Now define point  $b$  to be coincident with  $i$  at a particular time instant  $t_1$  identified as  $i(t_1)$ , and a line from  $a$  to  $i$  at that time. Further, define the  $a$ -to- $b$  line to be non-rotating so that as the gyro rotates,  $i$  will move away from  $b$ . At a time  $t_2$  later than  $t_1$ , point  $i$  will be at  $i(t_2)$ . The geometry is depicted in Fig. 1.

Now consider a photon  $p$  of light as it travels along the wave path, passing point  $b$  and  $i$  at  $t_1$  and travelling to its location at  $t_2$ , both identified in Fig. 1 as  $p(t_1)$  and  $p(t_2)$ .

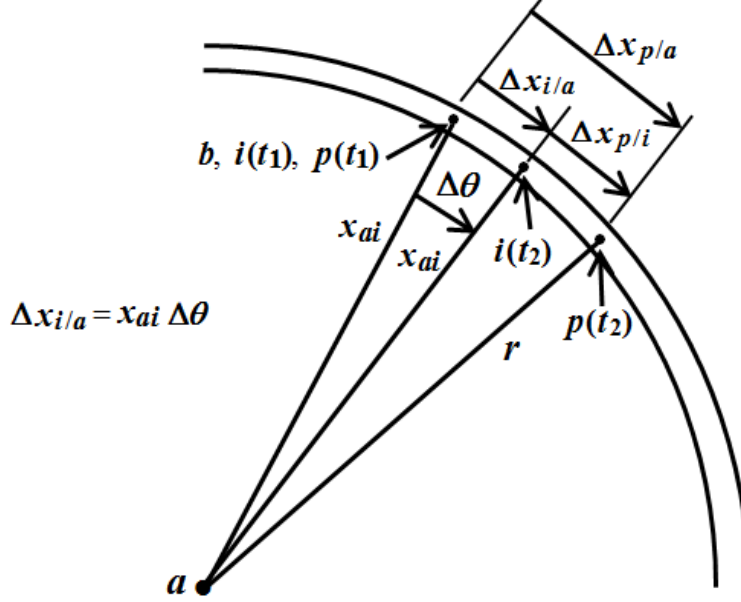


Fig. 1 Position Changes Along The Wave Path

Define  $\Delta x_{p/a}$  in Fig. 1 as the inertial distance movement of  $p$  along a perpendicular to the  $a$ -to- $b$  inertial line over the  $t_1$  to  $t_2$  interval, as observed at point  $a$  (on the  $a$ -to- $b$  line). Similarly,  $\Delta x_{i/a}$  in Fig. 1 is defined as gyro rotation induced point  $i$  movement from the  $a$ -to- $b$  inertial line as observed at point  $a$ , and  $\Delta x_{p/i}$  is the  $p$  point motion that would be observed at point  $i$  on the rotating gyro wave guide. Based on traditional Euclidean kinematics, Fig. 1 shows that the  $\Delta x_{p/a}$  photon motion observed at point  $a$  equates to  $p$  motion  $\Delta x_{p/i}$  observed at point  $i$  plus  $i$  motion  $\Delta x_{i/a}$  (induced by gyro rotation) observed at point  $a$ :

$$\Delta x_{p/a} = \Delta x_{p/i} + \Delta x_{i/a} \quad (1)$$

For a very small velocity of point  $i$  on the gyro relative to the speed of light, the appendix demonstrates that (1) is also compatible with Relativity kinematic theory.

Fig.1 also shows that the  $\Delta x_{i/a}$  distance in (1) can be represented by the equivalent  $x_{ai} \Delta\theta$  where  $\Delta\theta$  is a very very small inertial angular rotation of the gyro (and point  $i$ ) at distance  $x_{ai}$  from gyro wave guide center point  $a$  to point  $i$  on the wave path. Then (1) becomes

$$\Delta x_{p/a} = \Delta x_{p/i} + x_{ai} \Delta\theta \quad (2)$$

or equivalently,

$$\frac{\Delta x_{p/a}}{\Delta x_{p/i}} = 1 + \frac{x_{ai} \Delta\theta}{\Delta x_{p/i}} \quad (3)$$

Since (1) is compatible with both Euclidean and Relativity kinematic theory under normal operating conditions (as explained previously), (3) derived from (1), is also compatible with Euclidean and Relativity kinematic theory.

## WAVELENGTH EQUIVALENCE

Now consider that  $p$  represents a point in a monochromatic light wave travelling across the rotating  $a$ -to- $i$  line. Say that the  $\Delta x_{p/i}$  measurement initiates when the leading edge of the  $p$  wave passes that line and terminates when the leading edge of the next wave crosses the line. Then the  $p$  distance change  $\Delta x_{p/i}$  observed at point  $i$  will equal  $\lambda_{p/i}$ , the wavelength of the  $p$  wave as measured at point  $i$  and (3) becomes

$$\frac{\Delta x_{p/a}}{\lambda_{p/i}} = 1 + \frac{x_{ai} \Delta \theta}{\Delta x_{p/i}} \quad (4)$$

Note from (1), however, that the  $\Delta x_{p/a}$  measurement in (2) and (4) is independent of rotation (i.e., relative to point  $i$  motion), hence, it would be the same no matter the value of  $\Delta \theta$ . Thus, if we define  $\lambda_{0p}$  as the value of  $\lambda_{p/i}$  under zero  $\Delta \theta$ , we see from (4) that  $\Delta x_{p/a} = \lambda_{0p}$ , and (4) becomes:

$$\frac{\lambda_{0p}}{\lambda_{p/i}} = 1 + \frac{x_{ai} \Delta \theta}{\Delta x_{p/i}} \quad (5)$$

Finally, we define  $\Delta t_{p/i}$  to be the time interval for a  $p$  wave to translate through  $\Delta x_{p/i}$  across the  $a$ -to- $i$  line. For  $V_{p/i}$  defined as the  $p$  wave speed measured at point  $i$  we can write  $\Delta x_{p/i} = V_{p/i} \Delta t_{p/i}$ , and substitution in (5) finds

$$\frac{\lambda_{0p}}{\lambda_{p/i}} = 1 + \frac{x_{ai} \Delta \theta}{V_{p/i} \Delta t_{p/i}} \quad (6)$$

## THE EFFECT OF RELATIVITY

The derivations leading to (6) have been based on classical Euclidean kinematics. To continue we now incorporate a basic precept of Relativity theory; that the speed of a photon of light is the same constant  $c$  when measured at any point space. Thus, since  $V_{p/i}$  is the velocity of point  $p$  measured at point  $i$ , it follows that  $V_{p/i}$  will be  $c$ . Then (6) becomes

$$\frac{\lambda_{0p}}{\lambda_{p/i}} = 1 + \frac{x_{ai} \Delta\theta}{c \Delta t_{p/i}} \quad (7)$$

Now imagine a measuring tape attached to the gyro along the wave path, graduated in very fine increments for easy reading by an observer fixed to the gyro at point  $i$ . Additionally, consider a clock at point  $i$  to measure the time interval for any observed  $p$  location change (i.e.,  $\Delta\tau$ ). Over a small distance  $\Delta s$  measured along the tape by the  $i$  observer, the measured  $\Delta\tau$  time interval for a light wave to traverse  $\Delta s$  (at the speed of light  $c$ ) would be  $\Delta\tau = \Delta s / c$ . Thus,  $\Delta\tau$  would be the same for a light wave travelling through  $\Delta s$  in either direction at any point on the wave guide, regardless of whether or not the gyro is rotating, hence we can rewrite (7) as

$$\frac{\lambda_{0p}}{\lambda_{p/i}} = 1 + \frac{x_{ai} \Delta\theta}{c \Delta\tau} \quad (8)$$

The identical time/distance interval measurement for all waveguide mounted observers coupled with the wavelength change effect in (7) provides the mechanism for optical gyros to measure inertial angular rotation.

## OPTICAL GYRO OPERATION

Optical gyros create two oppositely directed but superimposed monochromatic light waves that traverse a closed-optical path, one (as before) identified as a  $p$  wave viewed from a point  $i$  in the waveguide, the oppositely directed wave as  $q$  viewed from a point  $j$  in the waveguide. Following the development approach for  $p$ , consider a non-rotating line from point  $a$  to a point  $b'$  in the gyro wave, point  $j$  in the wave path and photon  $q$  both coincident with  $b'$  at the start of  $\Delta\theta$  angular rotation. Then, accounting for  $q$  motion along the wave path being opposite from  $p$ , the equivalent to (1) and (2) for photon  $q$  would be:

$$\Delta x_{q/a} = \Delta x_{q/j} - \Delta x_{j/a} = \Delta x_{q/j} - x_{aj} \Delta\theta \quad (9)$$

where  $\Delta x_{q/a}$  is the magnitude of point  $q$  distance change relative to non-rotating space as viewed from point  $a$  (i.e., from the non-rotating  $a$ -to- $b'$  line at the start of the  $\Delta\theta$  angular rotation),  $\Delta x_{q/j}$  is the magnitude of  $q$  motion as viewed from point  $j$  on the rotating gyro (i.e., from a line from  $a$  to  $j$ ),  $\Delta x_{j/a}$  is the magnitude of  $j$  motion relative to non-rotating inertial space (i.e., from the  $a$ -to- $b'$  line), and  $x_{aj}$  is the distance from  $a$  to  $j$ . Following the procedure leading from (2) to (8), the equivalent for the  $q$  wave would be

$$\frac{\lambda_{0q}}{\lambda_{q/j}} = 1 - \frac{x_{aj} \Delta\theta}{c \Delta\tau} \quad (10)$$

where  $\lambda_{q/j}$  is the  $q$  light wave measured relative to the gyro at point  $j$  (during the  $\Delta\theta$  rotation),  $\lambda_{0q}$  is the  $\lambda_{q/j}$  wavelength that would be measured under zero  $\Delta\theta$  inertial rotation, and  $\Delta t_{p/b'}$  is time interval for  $\Delta\theta$  rotation as measured on a point  $b'$  located clock.

For this simplified analysis the wave path has been assumed circular so that  $x_{ai}$  and  $x_{aj}$  can be replaced by the circle radius  $r$  (see Fig. 1). Additionally, as will be justified subsequently for particular optical gyro configurations, the  $p$  and  $q$  wavelengths under zero angular rate will be the same  $\lambda_0$  value (i.e.,  $\lambda_{0q} = \lambda_{0p} = \lambda_0$ ). Based on these observations, (7) and (10) rearranged become for the  $p$  and  $q$  waves:

$$\frac{1}{\lambda_{p/i}} = \frac{1}{\lambda_0} \left( 1 + \frac{r \Delta\theta}{c \Delta\tau} \right) \quad \frac{1}{\lambda_{q/j}} = \frac{1}{\lambda_0} \left( 1 - \frac{r \Delta\theta}{c \Delta\tau} \right) \quad (11)$$

If we now let the  $\Delta$  changes in (11) become infinitesimally small  $d$  changes, (11) becomes the differential equivalent

$$\frac{1}{\lambda_{p/i}} = \frac{1}{\lambda_0} \left( 1 + \frac{r}{c} \omega \right) \quad \frac{1}{\lambda_{q/j}} = \frac{1}{\lambda_0} \left( 1 - \frac{r}{c} \omega \right) \quad \omega \equiv \frac{d\theta}{d\tau} \quad (12)$$

where  $\omega$  is the gyro angular rate relative to non-rotating inertial space.

## LIGHT WAVE EQUIVALENCE

Consider common point  $l$  where the “clockwise”  $p$  wave and “counterclockwise”  $q$  wave first enter the waveguide (at past time  $\tau = 0$ ). Further, consider point  $m$  in the “readout zone” on the waveguide at current time  $\tau = T$  where the  $p$  and  $q$  waves combine to generate an output measurement. For a sinusoidal  $p$  wave, the wave “height” at points  $l$  and  $m$  would be

$$g(T)_{p/l} = B \sin \phi(p, l) \quad g(T)_{p/m} = B \sin \phi(p, m) \quad (13)$$

where  $B$  is the  $p$  wave amplitude and  $\phi(p, l)$ ,  $\phi(p, m)$  are the wave front phases at points  $l$  and  $m$ .

Now consider two adjacent points along the waveguide between points  $l$  and  $m$ , points  $i$  and  $i_1$ , point  $i_1$  being an infinitesimally small distance  $ds_p$  from  $i$ . Further, consider that the distance between points  $l$  and  $i$  is the distance travelled by the  $p$  wave front at the speed of light  $c$  over time interval  $\tau$ , and that the distance travelled by the wave front over infinitesimally small time interval  $d\tau$  is  $ds_p$ . Then the  $p$  wave front phase  $\phi(p, i_1)$  at  $i_1$  will relate to  $\phi(p, i)$ , the phase at point  $i$  as

$$\phi(p, i_1) = \phi(p, i) + \frac{2\pi}{\lambda_{p/i}} ds_p = \phi(p, i) + \frac{2\pi}{\lambda_{p/i}} c d\tau \quad (14)$$

and the differential phase difference between points  $i$  and  $i_1$  over  $d\tau$  will be

$$d\phi(p, i) = \frac{2\pi c}{\lambda_{p/i}} d\tau \quad (15)$$

Beginning at  $\tau = 0$  at point  $l$ , the (15) differential can be accumulated (integrated) in the waveguide over a succession of  $i$  points from point  $l$  to point  $m$  (at time  $T$ ):

$$\phi(p, m) = \phi(p, l) + 2\pi c \int_{\tau=0}^{\tau=T} \frac{d\tau}{\lambda_{p/i}} \quad (16)$$

where (as before)  $\lambda_{p/i}$  is the wavelength of the  $p$  wave front when it reaches point  $i$  at time  $\tau$ , after its traversal from point  $l$  along the waveguide since  $\tau = 0$ . Substituting for  $\lambda_{p/i}$  from (12) then obtains

$$\phi(p, m) = \phi(p, l) + \frac{2\pi c}{\lambda_0} \int_{\tau=0}^{\tau=T} \left[ 1 + \frac{r}{c} \omega(\tau) \right] d\tau \quad (17)$$

where angular rate time dependence has now been more clearly delineated as  $\omega(\tau)$ . For the  $q$  wave, the equivalent of (13) – (17) would be

$$\phi(q, m) = \phi(q, l) + \frac{2\pi c}{\lambda_0} \int_{\tau=0}^{\tau=T} \left[ 1 - \frac{r}{c} \omega(\tau) \right] d\tau \quad (18)$$

$$g(T)_{q/l} = B \sin \phi(q, l) \quad g(T)_{q/m} = B \sin \phi(q, m)$$

Under accumulating differential rotation, (17) and (18) show that the  $p$  wave phase will increase and the  $q$  wave phase decrease by  $\frac{2\pi r}{\lambda_0} \int_{\tau=0}^{\tau=T} \omega(\tau) d\tau$ . The resulting phase difference in the gyro “readout zone” at time  $T$  provides the measurement of angular rotation for output.

## COMBINED OPPOSITELY DIRECTED WAVES IN THE READOUT ZONE

Now consider the wave height at point  $m$  at time  $\Delta\tau$ , a small time variation from time  $\tau = T$ . As both the  $p$  and  $q$  waves pass by point  $m$ , they will generate sinusoidal outputs at point  $m$  of the form

$$g(T+\Delta\tau)_{p/m} = B \sin \left[ \frac{2\pi}{\lambda_m} c \Delta\tau + \phi(p, m) \right] \quad g(T+\Delta\tau)_{q/m} = B \sin \left[ \frac{2\pi}{\lambda_m} c \Delta\tau + \phi(q, m) \right] \quad (19)$$

with  $\phi(p, m)$  and  $\phi(q, m)$  as defined in (17) and (18). Note: Eqs. (19) are based on the very good approximation that  $\Delta\tau$  is very small, thus, angular rate can be considered constant during  $\Delta\tau$ , and  $\lambda_m$  will also be approximate as constant - see (12) and note the very small dependence of  $\lambda$  on  $\omega$ .

Because the  $p$  and  $q$  waves occupy the same space in the waveguide at point  $m$ , their (19) wave functions at common “readout zone” point  $m$  will add at time  $\tau = T + \Delta\tau$  to form

$$\begin{aligned} h(T+\Delta\tau)_m &\equiv g(T+\Delta\tau)_{p/m} + g(T+\Delta\tau)_{q/m} \\ &= B \sin \left[ \frac{2\pi}{\lambda_m} c\Delta\tau + \phi(p, m) \right] + B \sin \left[ \frac{2\pi}{\lambda_m} c\Delta\tau + \phi(q, m) \right] \end{aligned} \quad (20)$$

or with (17) and (18):

$$\begin{aligned} h(T+\Delta\tau)_m &= B \sin \left\{ \frac{2\pi}{\lambda_m} c\Delta\tau + \phi(p, l) + \frac{2\pi}{\lambda_0} \left[ cT + r \int_{\tau=0}^{\tau=T} \omega(\tau) d\tau \right] \right\} \\ &\quad + B \sin \left\{ \frac{2\pi}{\lambda_m} c\Delta\tau + \phi(q, l) + \frac{2\pi}{\lambda_0} \left[ cT - r \int_{\tau=0}^{\tau=T} \omega(\tau) d\tau \right] \right\} \\ &= 2B \sin \frac{1}{2} \left\langle \left\{ \frac{2\pi}{\lambda_m} c\Delta\tau + \phi(p, l) + \frac{2\pi}{\lambda_0} \left[ cT + r \int_{\tau=0}^{\tau=T} \omega(\tau) d\tau \right] \right\} \right. \\ &\quad \left. \left\{ \frac{2\pi}{\lambda_m} c\Delta\tau + \phi(q, l) + \frac{2\pi}{\lambda_0} \left[ cT - r \int_{\tau=0}^{\tau=T} \omega(\tau) d\tau \right] \right\} \right\rangle \times \\ &\quad \cos \frac{1}{2} \left\langle \left\{ \frac{2\pi}{\lambda_m} c\Delta\tau + \phi(p, l) + \frac{2\pi}{\lambda_0} \left[ cT + r \int_{\tau=0}^{\tau=T} \omega(\tau) d\tau \right] \right\} \right. \\ &\quad \left. \left\{ -\frac{2\pi}{\lambda_m} c\Delta\tau - \phi(q, l) - \frac{2\pi}{\lambda_0} \left[ cT - r \int_{\tau=0}^{\tau=T} \omega(\tau) d\tau \right] \right\} \right\rangle \quad (21) \\ &= 2B \sin \left[ \frac{2\pi c}{\lambda_m} (T + \Delta\tau) + \frac{\phi(p, l) + \phi(q, l)}{2} \right] \cos \left[ \frac{\phi(p, l) - \phi(q, l)}{2} + \frac{2\pi r}{\lambda_0} \int_{\tau=0}^{\tau=T} \omega(\tau) d\tau \right] \end{aligned}$$

where  $h(\Delta\tau)_m$  is a combined  $p$  and  $q$  wave function at point  $m$  in the readout zone at time  $\tau = T + \Delta\tau$ . (Note: Eq. (38) assumes that the  $g(T+\Delta\tau)_{p/m}$  and  $g(T+\Delta\tau)_{q/m}$  functions lie in the same plane around the waveguide at the same instant of time and space, so that they add algebraically as shown. An important part of optical gyro design is based on meeting this requirement.)

The normalized power  $W(T+\Delta\tau)_m$  in the combined optical beam signal is proportional to the square of  $h(T+\Delta\tau)_m$  in (21):

$$W(T+\Delta\tau)_m \equiv \frac{h(\Delta\tau)_m^2}{B^2} \quad (22)$$

$$= 4 \sin^2 \left[ \frac{2\pi c}{\lambda_m} (T + \Delta\tau) + \frac{\phi(p,l) + \phi(q,l)}{2} \right] \cos^2 \left[ \frac{\phi(p,l) - \phi(q,l)}{2} + \frac{2\pi r}{\lambda_0} \int_{\tau=0}^{\tau=T} \omega(\tau) d\tau \right]$$

or with trigonometric expansion,

$$W(T+\Delta\tau)_m = \left\{ 1 - \cos \left[ \frac{4\pi c}{\lambda_m} (T + \Delta\tau) + \phi(p,l) + \phi(q,l) \right] \right\} \left\{ 1 + \cos \left[ \phi(p,l) - \phi(q,l) + \frac{4\pi r}{\lambda_0} \int_{\tau=0}^{\tau=T} \omega(\tau) d\tau \right] \right\} \quad (23)$$

Eq. (23) describes the power that would be measured by a photo detector located at point  $m$  in the waveguide at time  $t = T + \Delta t$ , being simultaneously illuminated by the  $p, q$  light beams. The power magnitude is modulated at high frequency by the first cosine term. For a typical optical gyro wavelength  $\lambda_m \approx \lambda_0$  of 0.63 microns (for a ring laser gyro), the modulation frequency  $2c/\lambda_m$  in the (40) cosine term is high enough ( $2 \times 3.0e8 / 0.63e-6 = 9.52 \text{ e}14 \text{ Hz}$ ) to be eliminated by attenuation in the photo-detector/readout electronics. Thus, (23) simplifies to

$$W(T)_m = 1 + \cos \left[ \phi(p,l) - \phi(q,l) + \frac{4\pi r}{\lambda_0} \int_{\tau=0}^{\tau=T} \omega(\tau) d\tau \right] \quad (24)$$

where  $W(T)_m$  is  $W(T+\Delta\tau)_m$  at time  $\tau = T$  (when  $\Delta\tau = 0$ ).

Eq. (24) is the basis for the design of both ring laser and fiber optic gyros. It demonstrates that optical gyros are integrating instruments whose combined optical beam power  $W(T)_m$  measures the integral of gyro input angular rate relative to non-rotating inertial space.

## RING LASER GYROS

A ring laser gyro (RLG) creates two oppositely directed beams of monochromatic light that traverse a closed optical path formed by three or more reflecting mirrors [7; 8]. The beams occupy the same physical space (“optical cavity”) and are constrained to travel along a fixed “waveguide” relative to the gyro by an aperture and curved surface mirror(s). The concept is depicted in Fig. 2 for a 3-mirror RLG configuration, the individual laser beams identified as travelling in the clockwise (cw) and counter-clockwise (ccw) directions.

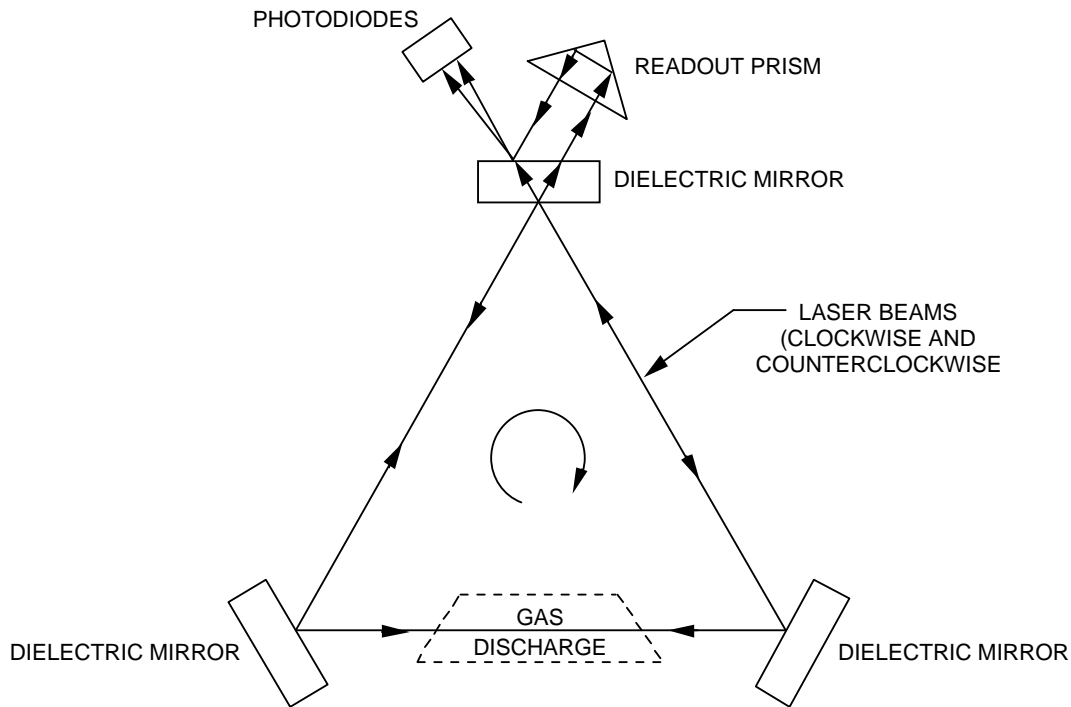


Fig. 2 - Ring Laser Gyro Operating Elements

The RLG light beams in Fig. 2 are sustained by the lasing action of a helium-neon gas discharge within the optical cavity. The reflecting surfaces are dielectric mirrors designed to selectively reflect the frequency associated with the particular helium-neon transition being used (typically of 0.63 micron wavelength). A small fraction of each beam escapes the cavity at the readout, one reflected through a corner prism, then recombined with the other on readout photo detectors (mounted in the gyro “readout zone”). The corner prism is designed to produce a small angle between the recombining beams, thereby creating optical interference fringes (light and dark bands) on the photo detectors, each illuminated by a different portion of the fringe pattern. The fringe pattern is stationary under zero angular rotation of the cavity. Under cavity rotation, the fringes move across the photo detectors, generating a sinusoidal output at a frequency proportional to the gyro angular rate around its input axis (perpendicular to the plane of the Fig. 2 diagram). Photo detector readout logic converts the sinusoidal output into a digital square wave for each fringe passage. The rise and fall of the square wave edges generate output pulses, each representing an angular rotation through a known angular increment (the gyro output pulse scale factor). Two photo detectors are used, separated from each other by one quarter of a photo-detector-sensed fringe so that resulting sinusoidal outputs are 90 deg phase separated. Comparison between photo detector generated square wave outputs determines the direction of rotation, positive or negative, depending on whether one square wave is leading or lagging the other.

Beam power losses in an RLG are compensated by amplification within the helium/neon plasma, adding photons at the same wavelength and in phase with returning photons (i.e., through Light Amplification by the Stimulated Emission of Radiation – LASER [7; 8]). When lasing is achieved, a returning wave at the same point in the waveguide will be in phase with

itself, and the total length of the closed wave path will contain an integral number of wavelengths. To sustain maximum beam power (average of the cw and ccw beams), the wave path is continuously adjusted through path length control (PLC), a closed-loop piezoelectric driven micro-movement of one of the RLG mirrors normal to its surface. Average beam power is measured for the PLC control loop by a separate photo detector mounted on one of the mirror substrates.

The amplification factor (“gain”) in a laser is a narrow Gaussian distribution function of light wave frequency (the “atomic gain curve”) centered at the nominal wavelength being excited by the Fig. 2 gas discharge (e.g., 0.63 microns for an RLG). An important part of RLG operation is control of the wavelength so that it coincides with the peak of the gain curve. (Operation away from the gain curve peak can produce complex deleterious performance effects that are beyond the scope of this article to explain. For very small RLGs, the impact can be large enough that there is insufficient gain for lasing.) When lasing frequency is at the gain curve peak, beam power is also maximized. Thus, PLC control to maximize beam power implicitly maintains operation at the gain curve peak, thereby stabilizing performance. An added benefit is maximizing illumination of the readout photo detectors, hence, improving output signal-to-noise ratio.

Under zero angular rotation, the RLG He-Ne stimulated emission process provides photons to both the clockwise and counterclockwise beams at their respective wavelengths, thus assuring that  $\lambda_{q/0} = \lambda_{p/0} = \lambda_0$ , the basic assumption in (11) leading to general optical gyro combined beam power equation (22) for RLG application. Under non-zero angular rotation, “Doppler broadening” within the He-Ne transition process [8] provides the mechanism for adding in-phase photons to returning  $p, q$  waves at their (12) shifted  $\lambda_{p/i}, \lambda_{q/j}$  wavelengths embedded in (24).

### RLG Analytical Model

The RLG He-Ne transition process generates new  $p$  and  $q$  oppositely travelling photons at the same phase and frequency as returning photons. This creates the illusion that each photon is repeatedly traversing the wave path. The result can be analytically represented by (24), a combined beam power input to the RLG photo detectors representing the integral of angular increments from the time the photons were initially created at lasing ignition. For an RLG waveguide in the shape of a triangle or regular polygon, [1] shows that (24) applies for  $r$  in that equation equated to the radius of the circle that can be inscribed within the triangle or regular polygon (i.e., tangent to each side). From [9 Eqs. 36 & 63], the inscribed circle radius is given by

$$\begin{aligned} \text{For a triangle: } r = r_{inscrb} &= \frac{1}{2} \sqrt{\frac{(b+c-a)(c+a-b)(a+b-c)}{a+b+c}} \\ \text{For a regular polygon: } r = r_{inscrb} &= \frac{S}{2 \tan(\pi/n)} \end{aligned} \quad (25)$$

where  $a, b, c$  are the lengths of the triangle sides,  $S$  is the length of any side of the regular polygon, and  $n$  is the number of regular polygon sides. Eq. (24) with  $r = r_{inscrb}$  then describes the combined RLG beam power  $W$  at point  $m$  in the Fig. 2 readout zone, with running time  $\tau = 0$  representing the time at gyro turn-on,  $\phi_{l/p_0} - \phi_{l/q_0}$  being the difference in phase between the Fig. 2 cw and ccw light beams at laser ignition, running time  $\tau = T$  representing current readout time since turn-on, and the integral being over the total time since laser ignition.

A fundamental distinction between an RLG and a FOG (to be described subsequently) is that in a FOG,  $\tau = 0$  represents a “computer controlled” time instant when an incremental angular output increment measurement begins, current time  $\tau = T$  represents the time the output measurement is made, and  $\tau = T$  also represents the time instant when the next angular incremental measurement begins. Sequential non-overlapping incremental measurements follow, each of duration  $T$ , the time for a wave front to travel along the fiber optic wave path from the input light emitting diode source to the output photo detector.

In contrast, for an RLG,  $\tau = 0$  represents the time of laser ignition, while  $\tau = T$  represents any time since laser ignition that the laser beams combine continuously in the readout zone. To distinguish this difference, we will equate  $T$  to general time interval  $t$  since laser ignition so that (24) becomes the revised form

$$W(t)_m = 1 + \cos \left[ \phi(p,l) - \phi(q,l) + \frac{4\pi r}{\lambda_0} \int_{\tau=0}^{\tau=t} \omega(\tau) d\tau \right] \quad (26)$$

As explained previously, the effect of (26) is to generate an optical interference pattern (“fringes”) across photo diodes in the gyro readout zone (Fig. 2). This can be analytically represented by first defining another point  $m'$  located in the readout zone, displaced from  $m$  by a small distance  $\Delta s$  “ahead” of  $m$  in the cw beam direction. At time  $t$ , the phase  $\phi(t)_{p/m'}$  of the clockwise  $p$  beam at point  $m'$  will equal the phase  $\phi(t)_{p/m}$  at  $m$  plus small distance  $\Delta s$  from  $m$  to  $m'$  measured in  $2\pi$  wavelengths, i.e.,  $\phi(t)_{p/m'} = \phi(t)_{p/m} + \frac{2\pi}{\lambda_m} \Delta s$  where  $\lambda_m$  is the cw light beam wavelength at point  $m$ . Similarly, the phase of the ccw beam (travelling in the opposite direction) will be reduced by the same amount:  $\phi(t)_{q/m'} = \phi(t)_{q/m} - \frac{2\pi}{\lambda_m} \Delta s$ . Then, incorporating the  $T \equiv t$  generalization, the equivalent to (13), (17) and (18) combined will be for point  $m'$

$$\begin{aligned} g(t)_{p/m'} &= B \sin \left\{ \phi(p,l) + \frac{2\pi}{\lambda_m} \Delta s + \frac{2\pi c}{\lambda_0} \int_{\tau=0}^{\tau=t} \left[ 1 + \frac{r}{c} \omega(\tau) \right] d\tau \right\} \\ g(t)_{q/m'} &= B \sin \left\{ \phi(q,l) - \frac{2\pi}{\lambda_m} \Delta s + \frac{2\pi c}{\lambda_0} \int_{\tau=0}^{\tau=t} \left[ 1 - \frac{r}{c} \omega(\tau) \right] d\tau \right\} \end{aligned} \quad (27)$$

where  $g(t)_{p/m'}$  and  $g(t)_{q/m'}$  are the  $p$  and  $q$  wave functions at space/time point  $m'(t)$ .

Following the same methodology that led from (18) to (24) then finds for the combined beam power at space/time point  $m'(t)$ :

$$W(t)_{m'} = 1 + \cos \left[ \phi(p,l) - \phi(q,l) + \frac{4\pi \Delta s}{\lambda_m} + \frac{4\pi r}{\lambda_0} \int_{\tau=0}^{\tau=t} \omega(\tau) d\tau \right] \quad (28)$$

Eqs. (28) and (26) represent general analytical models for the RLG combined beam power at points  $m$  and  $m'$ . Note that (28) and (26) are identical except for the  $4\pi \Delta s / \lambda_m$  phase shift in (28). At a given time  $t$ , (28) shows that normalized beam power  $W(t)_{m'}$  will vary sinusoidally across the readout zone, generating a repeating pattern of maximum/minimum values for each change in  $\Delta s$  by half a wavelength  $\lambda_m$ . This is an analytical representation of the previously described light/dark fringe pattern generated in the Fig. 2 RLG readout zone.

More importantly, for an RLG, (26) and (28) also show that the fringes will translate across the readout zone by the integral of angular rate  $\omega(\tau)$  as time  $t$  progresses into the future, repeating itself in time each time the  $\omega(\tau)$  weighted integral generates a specific integrated

angular rate increment, i.e., when  $\frac{2r}{\lambda_0} \int_{\tau=t}^{\tau=t+\Delta t} \omega(\tau) d\tau = 1$ , where  $\Delta t$  is the time increment when

the previous equality is true. Thus, for an optical photodiode pickoff located in the readout zone, angular rotation will generate a sinusoidal output, repeating each time the integrated angular rate accumulates that specific angular increment (the fundamental measurement “pulse size”).

Each output cycle represents a known increment of integrated angular rate along the gyro input axis. An output digitization process is implemented by first converting the analog sinusoidal pickoff output signal to an equivalent square wave, each change (minus to plus or plus to minus) indicating a gyro angular rotation of half the fundamental pulse size. The sign (plus or minus) of the rotation measurement is determined by adding a second photodiode at point  $m'$  in the readout zone, displaced from the one at point  $m$  by linear distance  $\Delta s$  to generate a of 90 deg ( $\pi/2$ ) phase shift from the  $m$  photodiode input. The length of  $\Delta s$  is analytically found from (28) by specifying  $4\pi \Delta s / \lambda_m = \pi / 2$  which finds  $\Delta s = \lambda_m / 8$ .

Generating a square wave from the  $m'$  diode creates a square wave that is 90 deg phase shifted from the  $m$  diode created square wave, the  $m'$  “states” (plus or minus) overlapping the state changes from the  $m$  square wave. Digital logic assigns a plus to the  $m$  sensed rotation when the  $m$  square wave state change finds a plus state on the  $m'$  square wave. Conversely, the rotation is negative when the  $m$  state change is accompanied by a negative  $m'$  state. Once the  $m$  and  $m'$  square wave measurements are implemented, the capability then exists to generate outputs not only for the  $m$  square wave state changes, but also for the  $m'$  square wave state changes. The method duplicates what was described for the  $m$  wave measurements, with the  $m'$  wave state change now used to indicate the rotation occurrence. Thus, 4 rotation occurrence outputs would be generated for each cycle of the photodiode outputs, 2 from the  $m$  wave, 2 from

the  $m'$  wave, all spaced one quarter of a wavelength apart, the equivalent of reducing the output “pulse size” by a factor of 4.

Eq. (26) or (28) with (25) can also be used to assess the RLG output scale factor for a particular waveguide geometry; triangle or regular polygon for the point  $m$  or  $m'$  photo detectors. For example, for a regular polygon, (26) with (25) shows that the normalized power at

a point  $m$  located photo detector will cyclically repeat each time  $\frac{S}{\lambda_0 \tan(\pi/n)} \int_{\tau=0}^{\tau=t} \omega(\tau) d\tau$

changes by 1, corresponding to an output “scale factor” of  $1 / \left[ \frac{S}{\lambda_0 \tan(\pi/n)} \right]$  radians change in

integrated angular rate change input  $\int_{\tau=0}^{\tau=t} \omega(\tau) d\tau$  per photo detector output cycle. For an

equilateral triangular RLG (i.e.,  $n = 3$ ) with  $S = 4.2$  inches per side (0.35 ft) and the commonly used visible RLG wavelength  $\lambda_0$  of 0.63 micron ( $2.02 \times 10^{-6}$  ft), the photo detector output scale factor will be

$$1 / \left[ \frac{S}{\lambda_0 \tan(\pi/n)} \right] = 1 / \left( \frac{0.35}{2.02 \times 10^{-6} \times 1.732} \right) = 1.00 \times 10^{-5} \text{ radians} = 2.06 \text{ arc sec per output cycle.}$$

By triggering two output pulses (one at each photo detector output half cycle) from each of the two photo detectors (being position phased in “quadrature” - 90 degrees apart as described previously), the combined output pulse scale factor would be  $2.06 / 4 = 0.515$  arc sec per pulse.

A square RLG configuration would have  $n = 4$ . For a scale factor equivalent to the previously described 4.2 inch per side triangular RLG, the square RLG would have

$$1 / \left[ \frac{S}{\lambda_0 \tan(\pi/n)} \right] = 1 / \left( \frac{S}{2.02 \times 10^{-6} \times 1.00} \right) = \frac{2.02 \times 10^{-6}}{S} = 1.00 \times 10^{-5} \text{ for which}$$

$S = 0.202 \text{ ft} = 2.42 \text{ inches} = 6.15 \text{ centimeters}$ , corresponding to a perimeter of 24.6 centimeters.

## FIBER-OPTIC GYROS

A fiber optic gyro (FOG) consists of a circular coil of optical fiber, the ends optically spliced together with fiber-optic couplers that route near-monochromatic light from a super-luminescent diode (e.g., gallium arsenide) into and out-of the coil [10 pp 186-190; 11; 12]. The concept is depicted in Fig. 3.

The light beam from the photo diode light source in Fig. 3 passes through a first coupler, then into the fiber-coil through a second coupler where it splits into two beams, one into the  $p$  branch, the other oppositely directed into the  $q$  branch. After traversing the coil, the beams recombine in the second coupler, and are gated through the first coupler to a readout photo detector. Under rotation, the  $p$  and  $q$  branch beams experience a relative phase shift, generating a change in the combined beam power illuminating the photo detector. Readout electronics convert the photo detector output into a measurement of angular rotation that created the phase shift.

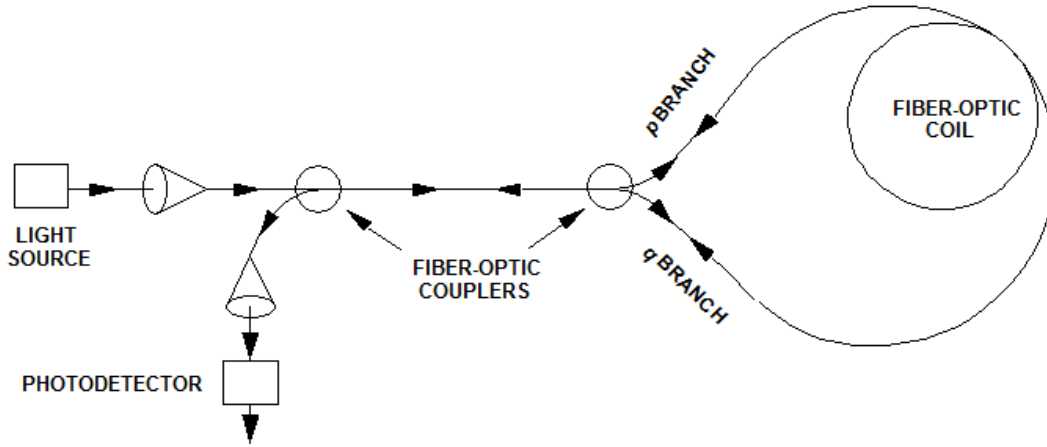


Fig. 3 - Fiber Optic Gyro (FOG) Concept

### Fundamental FOG Analytical Model

As with the RLG, the fundamental operation of a FOG can be represented by (24), describing the continuous light wave emitted from the diode light source in Fig. 3. For the FOG, the  $r$  radius in (24) can be approximated as the radius of the fiber coil.

For a FOG, each photon traverses the waveguide once from the photo-diode light source to the pickoff. Since the counter-travelling photons enter the waveguide at the same phase,  $\phi(p,l) - \phi(q,l)$  in (24) is zero. Thus, for the Fig. 3 FOG configuration, the general (24) analytical power model simplifies to

$$W(T)_m = 1 + \cos \left[ \frac{4\pi r}{\lambda_0} \Delta\theta(T) \right] \quad \Delta\theta(T) \equiv \int_{\tau=0}^{\tau=T} \omega(\tau) d\tau \quad (29)$$

where  $T$  is the time interval for a photon to traverse the fiber coil.

For a fiber length of 1,000 meters, the time for a photon to traverse the fiber coil at the speed of light ( $3 \times 10^8$  meters/sec) would be  $T = 1,000 / 3 \times 10^8 = 3.33 \times 10^{-6}$  sec. If the fiber coil is approximated as a connected set of  $n$  parallel overlapping circular segments, radius  $r$  in (29) would represent the approximate radius of each segment. If each circular segment has a 3 inch diameter (1.5 inch radius) and the light source wavelength  $\lambda_0$  is 0.82 microns (typical for a FOG gallium-arsenide photo-diode light source), under an average angular rate  $\omega(\tau)$  of 7 rad/sec (approximately 400 deg/sec), the bracketed (29) phase angle induced at the FOG pickoff would be  $\frac{4\pi r}{\lambda_0} \Delta\theta(t, T) = \frac{4\pi}{0.82 \times 10^{-6}} \times 1.5 \times 0.0254 \times 7 \times 3.33 \times 10^{-6} = 13.6$  rad.

To be useful for computing angular orientation in system applications, it is important that FOG output measurements of  $\Delta\theta(T)$  in (29) represent successive increments of angular change.

Then, using simultaneous outputs from three orthogonally mounted FOGs, they can be used effectively in an appropriate algorithm for repetitive three-dimensional attitude computation updating. Since each measurement of  $\Delta\theta(T)$  in (29) represents an attitude change over  $T$ , this means that  $\Delta\theta(T)$  measurements must be sampled and output at a frequency of  $1 / T$ . For  $T = 3.33 \text{ e-}6$  sec in the previous example, this translates into a  $\Delta\theta(T)$  measurement/sampling rate of  $1 / 3.33 \text{ e-}6 = 0.3$  mega-Hz.

### “Closed-Loop” FOG Configuration

A significant difference between the RLG and FOG arises in the complexity of the readout implementation. Most high accuracy mechanical gyros have been implemented in the past using narrow angle pickoffs designed to operate over a small angular input range (e.g., 1 milli-rad). The purpose is to minimize the effect of pickoff scale factor error on device performance, and is typically achieved by controlling the pickoff output in servo feedback fashion to dynamically maintain the pickoff output (hence, pickoff input) at zero (null). This has been achieved by either mechanically controlling the base to which the gyro is mounted (i.e., with a mechanical gimballed platform), or by using electrical “closed-loop” rebalance whereby an electrical signal is generated from the pickoff output to provide angular rate bias feedback within the gyro to maintain pickoff null [13]. A closed-loop gyro output would then be generated within the rebalance loop from the biasing signal required to maintain pickoff null, thereby becoming equal but opposite to the gyro dynamic angular input.

Eq. (29) illustrates the fundamental difficulty of measuring the scaled angular increment  $\Delta\theta(T)$  with an “open-loop” FOG; the lack of sensitivity in power  $W(T)$  for small  $\Delta\theta(T)$ , the inverse cosine function for  $\Delta\theta(T)$  becoming indeterminate at zero input rate, and prone to significant scale factor error (from pickoff output non-linearity characteristics) at non-zero angular increments. For a closed-loop FOG, the goal is to create closed-loop electrical bias that maintains  $W(T)$  at a known average value with high sensitivity for any value of  $\Delta\theta(T)$ . Thus, means must be introduced to enable measuring deviations from the specified average  $W(T)$  beam power, providing “closed loop” feedback to maintain  $W(T)$  at its specified average under all dynamic angular rate conditions.

For a closed-loop FOG, the equivalent to (29) also derives from (24), but having  $\phi(p,l)$  and  $\phi(q,l)$  include additional bias introduced within the fiber coil to enable closed-loop operation and  $\Delta\theta(T)$  determination under any input condition. Thus in (22),  $\phi(p,l)$  would equal  $\alpha + \Delta\beta_p$  and  $\phi(q,l)$  would equal  $\alpha + \Delta\beta_q$ , where  $\alpha$  is the phase of the light beam entering the coil (splitting into  $p$  and  $q$  branches as in Fig. 3), and  $\Delta\beta_p$ ,  $\Delta\beta_q$  represent additional phase biases intentionally introduced in the  $p$ ,  $q$  branches within the coil. The closed-loop equivalent to (29) then derives from (24) using the same rationale that led to (29):

$$\begin{aligned}
W(T)_m &= 1 + \cos \left[ \phi_{l/p_0} - \phi_{l/q_0} + \frac{4\pi r}{\lambda_0} \int_{\tau=0}^{\tau=T} \omega(\tau) d\tau \right] \\
&= 1 + \cos \left[ (\alpha + \Delta\beta_p) - (\alpha + \Delta\beta_q) + \frac{4\pi r}{\lambda_0} \int_{\tau=0}^{\tau=T} \omega(\tau) d\tau \right] \\
&= 1 + \cos \left( \Delta\beta_p - \Delta\beta_q + \frac{4\pi r}{\lambda_0} \Delta\theta(T) \right)
\end{aligned} \tag{30}$$

where  $\Delta\theta(T)$  is as defined in (29). Using condensed nomenclature, (30) becomes

$$W = 1 + \cos \left[ \Delta\phi + (\Delta\beta_p - \Delta\beta_q) \right] \quad \Delta\phi \equiv k_{SF} \Delta\theta(T) \quad k_{SF} \equiv \frac{4\pi}{\lambda_0} r \tag{31}$$

with  $r$  being the average fiber coil radius.

The FOG scale factor  $k_{SF}$  in (31) shows that there will be a  $\frac{4\pi}{\lambda_0} r$  radian shift in phase  $\Delta\phi$  between light waves reaching the readout photo detector per radian of  $\Delta\theta(T)$  angular rotation during time interval  $T$  for a photon to traverse the fiber coil. For comparison, (24) applied in (26) to an RLG with waveguide inscribed circular radius  $r$  shows that there would be a  $\frac{4\pi}{\lambda_0} r$

phase shift between light waves reaching the readout per radian change in  $\int_{\tau=0}^{\tau=t} \omega(\tau) d\tau$  integrated angular rate. Thus, both the FOG and RLG measure angular rotation changes by the same scale factor.

In modern day FOGs, integrated optics inserts are used to generate the  $\Delta\beta_p$  and  $\Delta\beta_q$  applied phase shifts in (31), based on the use of active electro-optic crystals that change the index of refraction of light passing through. With this approach, the integrated optics insert is constructed from a crystal of lithium-niobate using titanium strips diffused on the surface to gate light waves through the crystal [10 pp 189-190]. Voltage applied across the crystal changes the index of refraction of light passing through, changing the speed of light waves propagating through the crystal, thereby adding phase shift.

For a given applied voltage, the same phase shift will be added to waves entering from either side of the crystal, i.e., from the  $p$  or  $q$  wave directions in a FOG fiber coil. Achieving a net phase difference in (31) relies on the crystal being inserted at one end of the fiber to take advantage of the time interval difference for a  $p$  wave (for example) to reach the readout photo detector compared to the  $q$  wave. Thus, imagine a crystal inserted at the end of the coil where the  $p$  wave begins its journey. Then a voltage  $V_1$  (corresponding to a  $\beta_1$  phase shift) applied to the crystal at current time  $t_1$  will shift the  $p$  wave phase by  $\Delta\beta_p = \beta_1$ , but this shift will not appear on the photo detector until  $p$  completes its passage around the coil at a later time  $t_2$ .

Now consider a  $q$  wave that entered the coil with  $p$  at time  $t_1$ , but travelling in the opposite direction from  $p$  around the coil, and did not pass through the crystal until time  $t_2$ . If  $V_2$  is being applied to the crystal at time  $t_2$  (with corresponding phase shift  $\beta_2$ ), the  $q$  wave will be phase shifted by  $\Delta\beta_q = \beta_2$  when it reaches the photo detector at  $t_2$ . The net result is that at time  $t_2$ , the  $p$  and  $q$  waves with phase shifts  $\Delta\beta_p$  and  $\Delta\beta_q$  will combine on the photo detector to generate a phase shift difference  $\Delta\beta_p - \Delta\beta_q = \beta_1 - \beta_2$  in the (31) beam power, depending on the logic used in setting  $V_1$  and  $V_2$ . An example of applying this concept is depicted in Fig. 4, a closed-loop FOG version of Fig. 3.

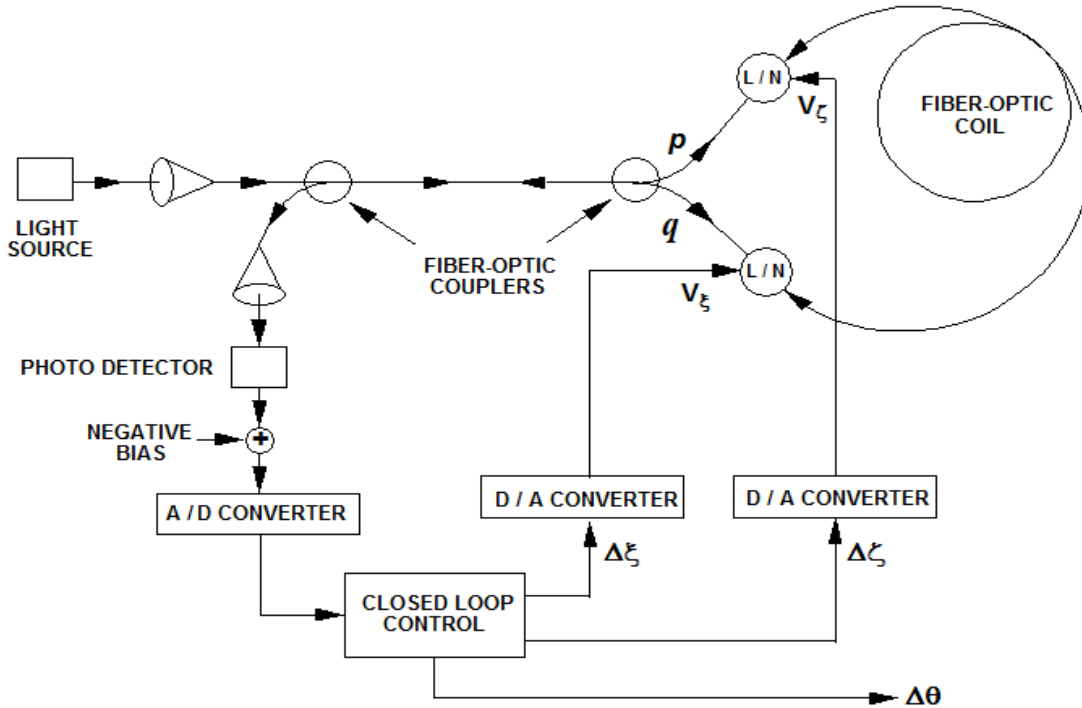


Fig. 4 – Closed-Loop FOG Configuration

A general goal in the design of inertial components is to provide symmetry to minimize the likelihood of asymmetric anomalous error generation. For a FOG, a symmetric design approach would use two lithium-niobate (L/N) crystals symmetrically placed in the  $p$  and  $q$  photon light paths at equal distances from the fiber coil junction, one located in the  $p$  branch, the other in the  $q$  branch. The symmetric configuration in Fig. 4 shows how the photo detector output would then be applied in feedback fashion through the Closed Loop Control computation block to generate  $\Delta\zeta$ ,  $\Delta\xi$  phase shifts in the  $p$ ,  $q$  waves through  $V_\zeta$ ,  $V_\xi$  voltages applied to the two L/N crystals. In conjunction with generating the  $\Delta\zeta$ ,  $\Delta\xi$  phase shift commands, Closed Loop Control in Fig. 4 also computes  $\Delta\theta$  angular increment measurements for output. The associated complex detail is provided in [1], the gist of which is summarized next.

The Closed Loop Control block in Fig. 4 generates the  $\Delta\zeta$ ,  $\Delta\xi$  phase shift commands and  $\Delta\theta$  output based on the biased A/D converted input from the photo detector. The purpose of the bias is to remove the “1” from the (31) power signal, converting the A/D power measurement to a cosine wave with plus/minus peak variations around zero. The  $\Delta\beta_p$ ,  $\Delta\beta_q$  phase biases in (31) are then designed to provide  $\widehat{\Delta\phi}$  feedback bias to balance the  $\Delta\phi$  input rotation generated phase shift. Simultaneously, the  $\Delta\beta_p$ ,  $\Delta\beta_q$  phases in (31) include  $\pi/2$  magnitude biases that alternate in polarity from one gyro output cycle to the next (each over the time for the  $p$ ,  $q$  waves to traverse the fiber coil). The alternating  $\pi/2$  bias converts the cosine to a sine function in (31), producing a power input  $W$  to the Closed Loop Control block of the cyclic form

$$W = \pm \sin(\Delta\phi - \widehat{\Delta\phi}) \approx \pm(\Delta\phi - \widehat{\Delta\phi}) \quad \Delta\phi \equiv k_{SF} \Delta\theta(t, T) \quad k_{SF} \equiv \frac{4\pi}{\lambda_0} r \quad (32)$$

Thus, unlike the lack of sensitivity of the open-loop power response in (29) under small  $\Delta\theta(t, T)$  rotation, closed-loop power input (32) has maximum sensitivity under all  $\Delta\theta(t, T)$  input rotations when the  $\widehat{\Delta\phi}$  feedback is accurately balancing  $\Delta\phi$ .

By subtracting the previous from the current power measurement in (32), the closed loop control error signal  $\Delta\phi - \widehat{\Delta\phi}$  is obtained, which is used to update the  $\widehat{\Delta\phi}$  rebalance signal for the next measurement cycle, and to provide  $\Delta\theta = \Delta\phi / k_{SF}$  outputs based on successfully balancing  $\Delta\phi$  with  $\widehat{\Delta\phi}$  (i.e., maintaining the  $\Delta\phi - \widehat{\Delta\phi}$  control loop error near zero so that  $\Delta\phi$  for output equals the average of  $\widehat{\Delta\phi}$ ). Third order corrections are included in [1] when generating  $\Delta\theta = \Delta\phi / k_{SF}$  to compensate small control loop variations in  $\Delta\phi - \widehat{\Delta\phi}$  from the nominal zero. Note that that the (32) cycle to cycle power subtraction process also cancels errors in the Fig. 4 analog bias on the A/D converter input from its nominal “1” value.

To assure that  $\Delta\zeta$ ,  $\Delta\xi$  values applied to the lithium-niobate (L/N) crystals in Fig. 4 remain positive (greater than a specified offset) and within a specified range for proper operation, successive plus or minus  $2\pi$  changes are applied to  $\Delta\zeta$ ,  $\Delta\xi$  until they satisfy the specified criteria. This also minimizes the maximum  $\Delta\zeta$ ,  $\Delta\xi$  range, hence, scale-factor/linearity error in the D/A to L/N crystal response branches. To minimize the effect of time delay between the  $\Delta\zeta$ ,  $\Delta\xi$  commands and D/A to L/N crystal response, the  $\Delta\zeta$ ,  $\Delta\xi$  commands are issued at the midpoint between successive  $W$  power measurements. Ref. [1] shows how to generate the  $\Delta\zeta$ ,  $\Delta\xi$  signals so that the previously described operations are shared equally by the two  $\Delta\zeta$ ,  $\Delta\xi$  branches. As a result, potential common bias errors created by thermal heating will be equal between the D/A – L/N group in each branch, thereby cancelling in the closed-loop computation process. Ref. [1] also describes how the Fig. 4 control loop can be structured to minimize digital round-off error in D/A converter sampling and generating the  $\Delta\theta$  digital-to-digital output function.

## CONCLUSIONS

Optical gyros generate oppositely directed monochromatic light waves travelling in a closed-circuit waveguide to measure angular rotation relative to non-rotating inertial space. Based on classical Euclidean kinematics and Relativity theory (under normal operating conditions), the wavelength of light waves in the waveguide will change due to angular rotation, increasing for waves travelling with rotation, decreasing for waves travelling against rotation. Due to Relativity theory, the velocity of the waves will remain constant (at the speed of light) relative to any point on the waveguide. As a result, relative to the readout device in the waveguide, the frequency will decrease for waves travelling with rotation, and increase for waves travelling against rotation. Additionally, relative to any point on the waveguide during rotation, the time increment for a wave to traverse a given distance increment will be the same, independent of its motion relative to the rotation direction. A corollary is that relative to the waveguide, the time interval for a wave to traverse a given distance will be the same for waves travelling in either direction.

Ring laser gyros (RLGs) and fiber optic gyros (FOGs) are integrating angular change sensing inertial instruments, both measuring increments of gyro angular rotation relative to non-rotating inertial space. The analytics describing RLG and FOG operations emanate from the same fundamental equation. RLGs and FOGs differ analytically in the method used to extract incremental angular data measurements for output. Application of the fundamental equation for each depends on the total travel time for a light wave to traverse the waveguide.

Due to the RLG He-Ne stimulated-emission process, a light wave in an RLG will continue to traverse the waveguide from gyro turn-on. The result is a pair of continuous counter-travelling light waves that combine at the readout, generating an optical interference pattern across the readout zone. The interference pattern moves across readout photo detectors at a rate proportional to the frequency difference between the counter-travelling light waves. The frequency difference is proportional to angular rate. The RLG output measures the occurrence of each interference pattern traversal, each representing a known increment of angular rotation relative to non-rotating inertial space.

In contrast, each light wave in a FOG only traverses the waveguide once from the time it leaves the FOG photo diode light source until it arrives at the readout photo detector. In a FOG, rotation generates a phase difference at the readout between the counter-travelling light waves. The phase difference is proportional to the increment of angular rotation during the time for a wave to traverse the waveguide. When the counter-travelling waves combine at the readout, the phase difference generates a change in the combined wave optical power illuminating the photo detector. Suitable closed-loop electronics convert photo detector optical power measurements into angular increments for output, while generating commands to lithium-niobate biasing crystal inserts in the gyro wave path for closed-loop control.

## APPENDIX

### DERIVATION OF EQ. (1) BASED ON RELATIVITY THEORY

For the simplified analysis presented here, assume that the observed motion of point  $p$  relative to points  $a$  and  $i$  are parallel along the  $x$  axis of a designated coordinate frame. Then the equivalent to (1) based on Relativity theory [5 Eq. (12-5); 6 Eq. (10.31) - (10.32)] in its equivalent point-to-point differential form [4 Eq. (35)] would be:

$$dx_{p/i} = \frac{1}{\sqrt{1 - v_{ai}^2/c^2}} (dx_{p/a} - v_{i/a} dt_a) \quad dy_{p/i} = dy_{p/a} \quad dz_{p/i} = dz_{p/a} \quad (\text{A-1})$$

where  $dx_{p/a}$ ,  $dy_{p/a}$ ,  $dz_{p/a}$  are differential changes in the  $x, y, z$  position location components of point  $p$  as observed at point  $a$ ,  $dx_{p/i}$ ,  $dy_{p/i}$ ,  $dz_{p/i}$  are differential position changes of  $p$  as observed at point  $i$ ,  $dt_a$  is the time interval for  $p$  position change that would be measured on a point  $a$  located clock,  $v_{i/a}$  is the velocity of point  $i$  relative to point  $a$ , and  $v_{ai}$  is the magnitude of  $v_{i/a}$ . The peculiar  $\sqrt{1 - v_{ai}^2/c^2}$  term in (A-1) is a unique contribution from Relativity theory [4; 14 Appendix A] that assures that if point  $p$  is travelling at the speed of light  $c$ , the magnitude of  $p$  velocity relative to observation points  $a$  or  $i$  will be the same  $c$  constant:

$$\left| dx_{p/a} / dt_a \right| = \left| dx_{p/i} / dt_i \right| = c \quad (\text{A-2})$$

where  $dt_i$  is the time interval for the  $dx_{p/i}$  differential  $p$  motion that would be measured on a clock located at point  $i$ .

Eq. (A-1) is also based on  $v_{a/i}$  (the velocity of point  $a$  observed at point  $i$ ) being of equal magnitude but oppositely directed from  $v_{i/a}$  (the velocity of point  $i$  observed at point  $a$ ), a fundamental premise of both classical Euclidean kinematics and Relativity theory [3 pp 236-238; 6 pp 30]:

$$v_{i/a} \equiv \frac{dx_{i/a}}{dt_a} \quad v_{a/i} \equiv \frac{dx_{a/i}}{dt_i} \quad v_{a/i} = -v_{i/a} \quad v_{ai} \equiv |v_{i/a}| = |v_{a/i}| \quad (\text{A-3})$$

For the commonly encountered situations when  $v_{ai} \ll c$ , the  $\sqrt{1 - v_{ai}^2/c^2}$  Relativity coefficient in (A-1) approximates as unity and (A-1) simplifies to

$$dx_{p/i} = dx_{p/a} - v_{i/a} dt_a \quad (\text{A-4})$$

Substituting  $dx_{i/a} = v_{i/a} dt_a$  from (A-3) into (A-4) obtains with rearrangement

$$dx_{p/a} = dx_{p/i} + dx_{i/a} \quad (\text{A-5})$$

With the differentials in (A-5) approximated as small finite  $\Delta$  changes, (A-5) becomes (1) in the main text based on classical Euclidean kinematic theory:

$$\Delta x_{p/a} = \Delta x_{p/i} + \Delta x_{i/a} \quad (\text{A-6})$$

## ACKNOWLEDGMENT

I would like to express my appreciation to Ted Podgorski, a key design engineer in the evolutionary development of RLGs at Honeywell, for his advice when preparing the Ring Laser Gyros section of this article.

## REFERENCES

- [1] Savage, P. G., “Analytical Description of Optical Gyros”, SAI WBN-14024, Apr 23, 2019, Updated (November 6, 2022 and March 15, 2024), free access available at [www.strapdownassociates.com](http://www.strapdownassociates.com).
- [2] Einstein, A., *Relativity, The Special and the General Theory*, 1961, The Estate of Albert Einstein.
- [3] Born, Max, *Einstein’s Theory of Relativity*, Dover Publications, Inc., New York.
- [4] Savage, P. G., “Differential Kinematics Of Point-To-Point Relativity”, SAI WBN-14021, March 11, 2018, free access available at [www.strapdownassociates.com](http://www.strapdownassociates.com).
- [5] Halfman, Robert L., *Dynamics: Systems, Variational Methods, Relativity, Volume II*, Addison-Wesley, 1962.
- [6] Fock, V., *Theory of Space, Time, and Gravitation, Second Revised Edition*, New York: Pergamon Press, 1964.
- [7] Killpatrick, Joseph, "The Laser Gyro", IEEE Spectrum, Oct. 1967.
- [8] Aronowitz, F., “Fundamentals of the Ring Laser Gyro”, Paper 3., *Optical Gyros And Their Applications*, NATO RTO-AG-339, May 1999.
- [9] Burington, R. S., *Handbook Of Mathematical Tables And Formulas*, R. S. Burington, 1933 – 1948, Handbook Publishers, Inc. Sandusky, OH
- [10] Lawrence, A., *Modern Inertial Technology*, Springer-Verlag 1993.

- [11] Lefevre, C. L., “Application Of The Sagnac Effect In The Interferometric Fiber-Optic Gyroscope”, Paper 7, *Optical Gyros And their Applications*, NATO RTO-AG-339, May 1999.
- [12] Ezekiel, S. and Arditty, H.J., ed. *Fiber Optic Rotation Sensors and Related Technologies*, Springer-Verlag, Berlin/Heidelberg/New York, 1982.
- [13] Savage, P.G., “Blazing Gyros – The Evolution of Strapdown Inertial Navigation Technology For Aircraft”, *AIAA Journal Of Guidance, Control, And Dynamics*, Vol. 36, No. 3, May - June, 2013, pp. 637-655, also posted for free-access as WBN-14009 at [www.strapdownassociates.com](http://www.strapdownassociates.com).
- [14] Savage, P. G., “Differential Point-To-Point Relativity In Rotating Coordinates”, SAI WBN-14022, May 28, 2018, free access available at [www.strapdownassociates.com](http://www.strapdownassociates.com).